AIAA JOURNAL
Vol. 46, No. 6, June 2008

Smart Double Panel with Decentralized Active Dampers for Sound Transmission Control

Neven Alujević,* Paolo Gardonio,† and Kenneth D. Frampton‡
University of Southampton, Southampton, England SO17 1BJ, United Kingdom

DOI: 10.2514/1.32369

This paper presents a theoretical study of decentralized velocity feedback control systems for the reduction of sound transmission through double panels. The system studied consists of two plates which are coupled acoustically by the air in the cavity between them and structurally by four elastic mounts. The geometrical and material properties of the double panel have been chosen so as to approximate a section of an aircraft fuselage skin. The outer panel of the skin (the source panel) is excited by oblique plane waves and the consequent sound power radiated from the inner panel (the radiating panel) is calculated. First, a parametric study of passive sound transmission of double panels with different geometrical and material properties is carried out. Second, active vibration control is implemented using 16 decentralized direct velocity feedback loops. Performance of such a control system is assessed for four control cases. The first two cases deal with skyhook force actuators with collocated velocity sensors, which implement active damping either on the source panel or on the radiating panel. In the third case, skyhook actuators and collocated velocity sensors are located on both panels. Finally, an approach using actuators that react between the two panels with collocated relative velocity sensors is considered.

I. Introduction

THE construction of air transportation vehicles such as aircraft or helicopters typically involves a considerable number of thin-walled structural elements. From the vibroacoustic point of view, such a structure is naturally characterized by relatively low levels of damping, and in such cases, noise and vibration issues become increasingly important [1]. These vibration and noise problems are traditionally solved by passive means [2,3]. For example, the resonance effect can be reduced by increasing the damping with dissipative treatments. Alternatively, the response of the structure can be influenced by changing mass and stiffness properties to avoid excessive excitation of the most efficient radiating modes. Finally, special designs can be used, such as double panel constructions. For example, a typical passenger compartment of a civil aircraft is equipped with an inner shell of nonmetallic, lightweight material (i.e., a trim panel). Thus, a thin air cavity is formed between the trim panel and the outer skin. The cavity is commonly filled with high density fiberglass blankets primarily for the improvement of thermal insulation. These insulation layers have the added benefit of increasing the vibration damping and high-frequency noise attenuation of the double panel system [4]. Additionally, in contrast to a single skin vibroacoustic system, the sound power transmission ratio of such a double panel decreases steeply above the mass–air–mass resonant frequency, where the sound transmission is governed by mass law [5].

However, in passenger transport vehicles, noise sources tend to cover a broad frequency band [1]. Thus, they substantially excite the structure at low frequencies below the cutoff frequency, where the mass law starts governing the transmission of sound, and below the frequencies at which the passive treatments are effective. For example, the primary contributor to jet aircraft interior noise under cruising conditions is the turbulent boundary layer (TBL) [1]. Under typical cruise conditions, the excitation spectrum generated by TBL pressure fluctuations is most significant between 100 and 2000 Hz [6]. Because the passive treatments (high-density fiberglass blankets) are only effective at higher audio frequencies, the sound at lower audio frequencies is efficiently transmitted through the double fuselage skin.

A possible solution to the low-frequency noise transmission problem is active control [7,8]. This paper is focused on the application of active vibration control (AVC) to reduce the low-frequency noise transmission through a typical aircraft double panel. Active control could reduce the sound transmission in the lower frequency range, whereas higher frequency passive sound transmission loss is enhanced by the mass law that governs the response of the double panel.

Active control systems can be divided into two groups: feedforward and feedback control systems. Feedforward control approaches require that a reference signal, correlated to the primary disturbance, be known far enough in advance that a causal control filter can be designed [9,10]. Normally, this is possible for tonal disturbances, although it is rather difficult for random disturbances. In particular, it is very difficult to implement when disturbances are randomly distributed in both time and space (for example, diffuse sound fields or turbulent boundary-layer excitation). In such a case, feedback control systems should be used.

The control of broadband random disturbances acting on distributed systems requires multi-input/multi-output (MIMO) feedback control. Fully coupled (centralized) MIMO systems require a reliable model of the response functions between all control sensors and actuators [11,12], and thus are difficult to implement in practice. However, Petitjean and Legrain have shown that, for a thin panel with a 5×3 array of piezoelectric patch sensor-actuator pairs, a decentralized MIMO control gives results very similar to those of a fully coupled MIMO control system [13]. Furthermore, using direct velocity feedback loops in a decentralized MIMO system, active damping [14] can be generated: a feature that improves passive damping in the low-frequency range [15]. Thus, the low-frequency resonant response of thin panels can be successfully reduced [15,16]. Provided that control gains are optimally adjusted (too high gains tend to pin the plate at the control position [16,17]), both vibratory kinetic energy and sound radiation can be reduced. A decentralized MIMO velocity feedback system is unconditionally stable if the sensor/actuator pairs are dual and collocated [18,19], as is the case with collocated ideal point force actuators and ideal velocity sensor pairs [16]. The problem is, however, that the force actuators cannot

Received 26 May 2007; accepted for publication 22 November 2007.

*Research Student, Institute of Sound and Vibration Research.
†Professor of Systems Dynamics and Control, Institute of Sound and Vibration Research.
‡Senior Lecturer, Institute of Sound and Vibration Research.

act without reacting off another body. For that reason, other types of actuators, such as strain actuators or proof mass (inertial) actuators are often used in decentralized MIMO control systems, although they do not guarantee the collocation and duality properties [20–24].

In this paper, decentralized active damping systems are applied to a double panel. The physics of the double panel sound transmission, as well as the control system performance, are the focus of the study. The paper is organized in four sections. Section II presents the double panel modeling problem and the mathematical approach used. Section III discusses a parametric study of passive sound transmission. This includes the effects on sound transmission of the radiating panel mass and stiffness, the cavity depth and the structural mounting system stiffness. The fourth section is concerned with active control using 16 direct velocity feedback units. Performance of this control approach is assessed for four cases. The first two cases deal with skyhook force actuators and collocated velocity sensors, which implement active damping either on the source panel or on the radiating panel. In the third case, skyhook actuators and collocated velocity sensors are located on both panels. Finally, the fourth case considers actuators that react off the two panels with collocated relative velocity sensors.

II. Model Problem

A. Smart Double Panel

The double panel considered in this study consists of two finite plates, shown in Fig. 1, that are structurally coupled via elastic mounts and acoustically coupled through the air in the cavity between the plates.

The source panel is excited by an acoustic plane wave, while the radiating panel radiates sound into a free field. The source panel is simply supported along all the edges to approximate a panel attached to a rigid structure. The source panel is modeled as a $414 \times 314 \times 1$ mm aluminum panel, representative of a section of the outer skin of a typical civil aircraft. To excite all the vibratory modes of the source panel, the acoustic plane wave excitation has azimuthal and elevation incidence angles of 45 deg. The radiating panel is modeled as a plate with free boundary conditions along the four edges, structurally connected to the source panel by four rubber mounts. The radiating panel has the same x and y dimensions as the source panel, but it is made of a honeycomb composite material 3 mm thick. These properties have been chosen so as to emulate a typical civil aircraft trim panel. As shown in Fig. 1, the double panel is equipped with a 4×4 array of collocated reactive point force actuators and velocity sensors which can be used to generate relative velocity feedback between the two panels. In addition, ideal skyhook force actuators with collocated velocity sensors, located on either the source or radiating panel, are considered in this paper. The array of decentralized control system elements have been equally spaced along the x and y directions in such a way that the distances between actuators (sensors) are equal to the distance between the edge of the plate and a perimeter actuator (sensor).

B. Mathematical Model

A mobility matrix model [25] is used in the double panel vibro-acoustic simulation. The mobility model assumes that the system is divided into three components: the source panel, the radiating panel, and the structure-borne and airborne sound transmission paths. The structure-borne transmission path is given by the sound transmission via the elastic mounts, whereas the airborne path is due to the sound transmission via the air confined between the radiating and the source panel. Each of these system components is modeled using point and transfer mobility or impedance functions. The airborne transmission path is modeled using transfer impedances between a finite number of cavity elements that are adjacent to the surfaces of the panels. The excitation of the source panel by the incident acoustic wave and the radiated sound power from the radiating panel are calculated by assuming that the two panels are divided into the same number of elements. This number is obtained by choosing element dimensions $l_{x,e} = l_x/(4M)$ and $l_{y,e} = l_y/(4N)$, where M and N are the highest modal indices used in calculations. The mobility model is shown schematically in Fig. 2.

The model considers only out-of-plane displacements/velocities and forces at the various junctions and at the centers of the plate and cavity elements. The time-harmonic displacement or force functions are given by $w(t) = Re\{w(\omega)e^{j\omega t}\}$ or $f(t) = Re\{f(\omega)e^{j\omega t}\}$, where ω is the circular frequency in [rad/s], and $w(\omega)$ and $f(\omega)$ are the complex frequency-dependent displacement and force phasors. To simplify the formulation used in this paper, the time-harmonic

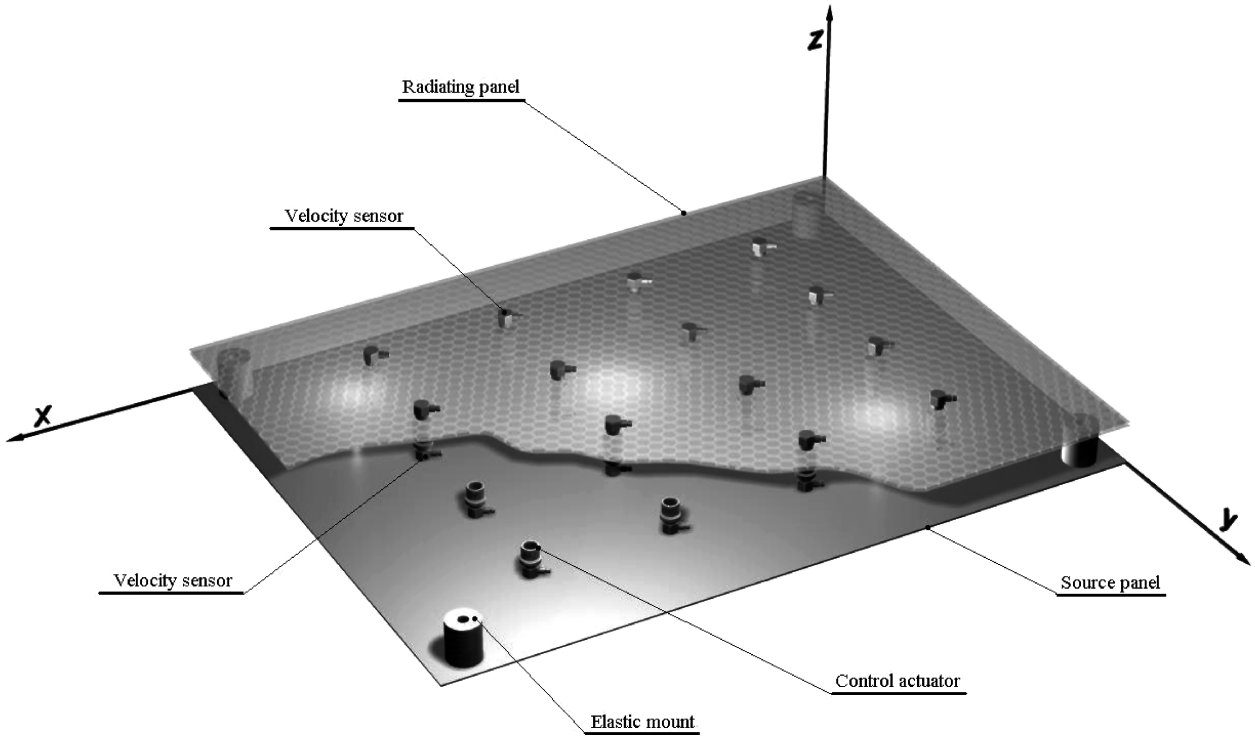

Fig. 1 Smart double panel.

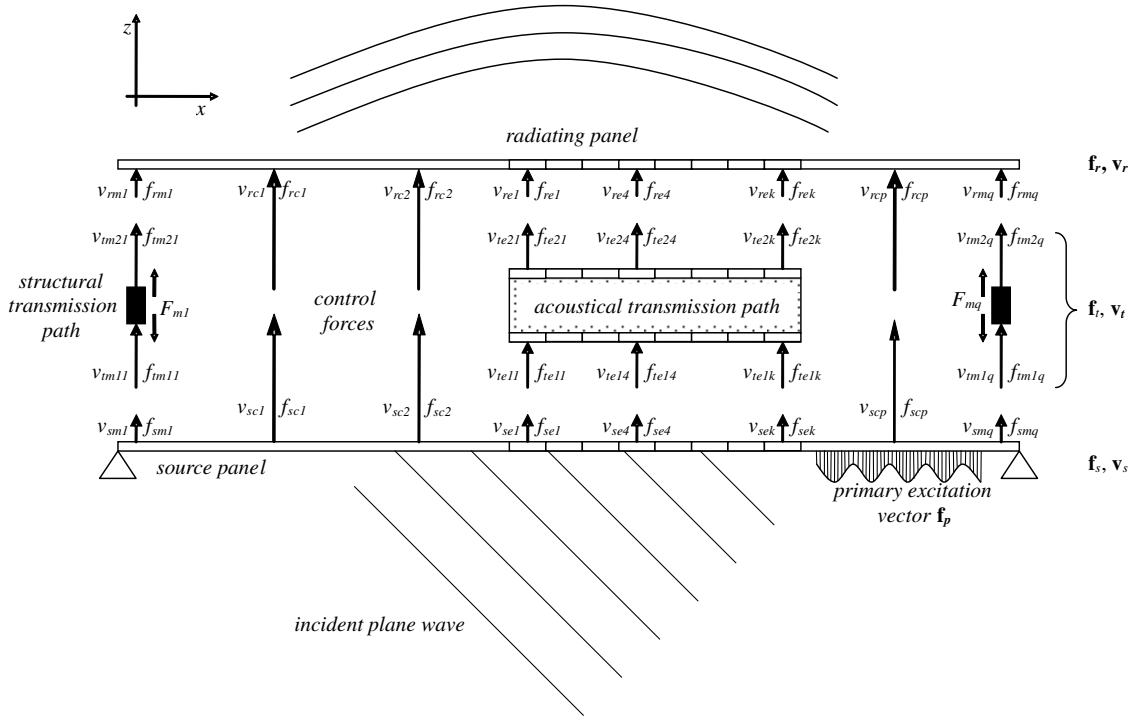

Fig. 2 Mobility model scheme.

dependence is implicitly assumed in the mathematical expressions, which are therefore formulated in terms of the frequency-dependent phasors. Also, the first and second derivative of the time-harmonic functions, for example, the linear out-of-plane velocity $\dot{w}(t) = Re\{j\omega w(\omega)e^{j\omega t}\}$ or linear out-of-plane acceleration $\ddot{w}(t) = Re\{-\omega^2 w(\omega)e^{j\omega t}\}$, are represented by velocity and acceleration frequency-dependent phasors $\dot{w}(\omega) = j\omega w(\omega)$ and $\ddot{w}(\omega) = -\omega^2 w(\omega) = j\omega\dot{w}(\omega)$.

The transmission path through the elastic mounts is modeled as an elastic out-of-plane force, so that point impedances can be used to model the coupling at the mount locations. The equations are developed assuming an arbitrary number of mounts. However, subsequent analysis considers only $q = 4$ elastic mounts. These four mounts are attached to the two panels near the plate corners, as is usually the case with aircraft trim panel mounting systems. At each mount junction, the motion and the transmitted forces are characterized by a complex function that corresponds to the out-of-plane z translational degree of freedom. Other vibration degrees of freedom, such as in-plane displacements or out-of-plane rotations, are neglected in this model [25].

The velocity and force phasors at the mount locations are grouped in the following column vectors:

$$\boldsymbol{v}_m \equiv \{\dot{w}_1, \dot{w}_2, \ldots \dot{w}_j, \ldots \dot{w}_{q-1}, \dot{w}_q\}^T \tag{1}$$

$$\boldsymbol{f}_m \equiv \{N_{z1}, N_{z2}, \ldots N_{zj}, \ldots N_{zq-1}, N_{zq}\}^T \tag{2}$$

where $\dot{w}_j$ is the complex amplitude of the linear velocity along the z axis and N_{zj} is the complex amplitude of the force in the z direction at the j-th elastic mount.

The two panels are also excited by means of p control forces. The velocity and control force phasors at the control positions in the source and radiation panels are grouped in the following two column vectors:

$$\boldsymbol{v}_c \equiv \{\dot{w}_1, \dot{w}_2, \ldots \dot{w}_j, \ldots \dot{w}_{p-1}, \dot{w}_p\}^T \tag{3}$$

$$\boldsymbol{f}_c \equiv \{N_{z1}, N_{z2}, \ldots N_{zj}, \ldots N_{zp-1}, N_{zp}\}^T \tag{4}$$

The double panel is also characterized by an acoustical transmission path due to the air in the cavity between the two plates. As shown in Fig. 2, the cavity boundaries along the source and the radiating plates are modeled using k elements whose dimensions are much smaller than the shortest acoustic wavelength in the cavity, and smaller than the shortest structural wavelength in the plate for the frequency range considered. The sides of the air cavity are assumed to be rigid walls; thus, the air cavity is assumed to be sealed. The top and bottom surface elements velocities and forces are defined at the geometrical center of each element.

The velocity and force phasors for each element are grouped in the following two column vectors:

$$\boldsymbol{v}_e \equiv \{\dot{w}_1, \dot{w}_2, \ldots \dot{w}_j, \ldots \dot{w}_{k-1}, \dot{w}_k\}^T \tag{5}$$

$$\boldsymbol{f}_e \equiv \{N_{z1}, N_{z2}, \ldots N_{zj}, \ldots N_{zk-1}, N_{zk}\}^T \tag{6}$$

With reference to the notation shown in Fig. 2, the six vectors are grouped together to form four combined vector pairs. These four groups are as follows: the source velocity vector $\boldsymbol{v}_s$ and the source force vector $\boldsymbol{f}_s$; the radiating velocity vector $\boldsymbol{v}_r$ and the radiating force vector $\boldsymbol{f}_r$; the transmission system velocity vector $\boldsymbol{v}_t$ and the transmission system force vector $\boldsymbol{f}_t$; and finally, the control velocity vector $\boldsymbol{v}_c$ and the control force vector $\boldsymbol{f}_c$. The four groups of vectors are given by

$$\boldsymbol{v}_s \equiv \begin{Bmatrix} \boldsymbol{v}_{sm} \\ \boldsymbol{v}_{se} \end{Bmatrix} \equiv \begin{Bmatrix} v_{sm1} \\ v_{sm2} \\ \vdots \\ v_{smq} \\ v_{se1} \\ v_{se2} \\ \vdots \\ v_{sek} \end{Bmatrix} \tag{7}$$

$$\boldsymbol{v}_r \equiv \begin{Bmatrix} \boldsymbol{v}_{rm} \\ \boldsymbol{v}_{re} \end{Bmatrix} \equiv \begin{Bmatrix} v_{rm1} \\ v_{rm2} \\ \vdots \\ v_{rmq} \\ v_{re1} \\ v_{re2} \\ \vdots \\ v_{rek} \end{Bmatrix} \tag{8}$$

$$\boldsymbol{v}_t \equiv \begin{Bmatrix} \boldsymbol{v}_{tm1} \\ \boldsymbol{v}_{te1} \\ \boldsymbol{v}_{tm2} \\ \boldsymbol{v}_{te2} \end{Bmatrix} \equiv \begin{Bmatrix} v_{tm11} \\ \vdots \\ v_{tm1q} \\ v_{te11} \\ \vdots \\ v_{te1k} \\ v_{tm21} \\ \vdots \\ v_{tm2q} \\ v_{te21} \\ \vdots \\ v_{te2k} \end{Bmatrix} \tag{9}$$

$$\boldsymbol{v}_c \equiv \begin{Bmatrix} \boldsymbol{v}_{sc} \\ \boldsymbol{v}_{rc} \end{Bmatrix} \equiv \begin{Bmatrix} v_{sc1} \\ v_{sc2} \\ \vdots \\ v_{scp} \\ v_{rc1} \\ v_{rc2} \\ \vdots \\ v_{rcp} \end{Bmatrix} \tag{10}$$

$$\boldsymbol{f}_s \equiv \begin{Bmatrix} \boldsymbol{f}_{sm} \\ \boldsymbol{f}_{se} \end{Bmatrix} \equiv \begin{Bmatrix} f_{sm1} \\ f_{sm2} \\ \vdots \\ f_{smq} \\ f_{se1} \\ f_{se2} \\ \vdots \\ f_{sek} \end{Bmatrix} \tag{11}$$

$$\boldsymbol{f}_r \equiv \begin{Bmatrix} \boldsymbol{f}_{rm} \\ \boldsymbol{f}_{re} \end{Bmatrix} \equiv \begin{Bmatrix} f_{rm1} \\ f_{rm2} \\ \vdots \\ f_{rmq} \\ f_{re1} \\ f_{re2} \\ \vdots \\ f_{rek} \end{Bmatrix} \tag{12}$$

$$\boldsymbol{f}_t \equiv \begin{Bmatrix} \boldsymbol{f}_{tm1} \\ \boldsymbol{f}_{te1} \\ \boldsymbol{f}_{tm2} \\ \boldsymbol{f}_{te2} \end{Bmatrix} \equiv \begin{Bmatrix} f_{tm11} \\ \vdots \\ f_{tm1q} \\ f_{te11} \\ \vdots \\ f_{te1k} \\ f_{tm21} \\ \vdots \\ f_{tm2q} \\ f_{te21} \\ \vdots \\ f_{te2k} \end{Bmatrix} \tag{13}$$

$$\boldsymbol{f}_c \equiv \begin{Bmatrix} \boldsymbol{f}_{sc} \\ \boldsymbol{f}_{rc} \end{Bmatrix} \equiv \begin{Bmatrix} f_{sc1} \\ f_{sc2} \\ \vdots \\ f_{scp} \\ f_{rc1} \\ f_{rc2} \\ \vdots \\ f_{rcp} \end{Bmatrix} \tag{14}$$

where v_{smj}, f_{smj}, and v_{sej}, f_{sej} represent the complex velocities and forces at the source junction for the jth mount and the jth acoustic element; v_{rmj}, f_{rmj}, and v_{rej}, f_{rej} represent the complex velocities and forces at the radiating junction for the jth mount and the jth acoustic element; v_{tm1j}, f_{tm1j}, and v_{te1j}, f_{te1j} represent the complex velocities and forces for the jth mount and for the jth acoustic element on the source panel; v_{tm2j}, f_{tm2j}, and v_{te2j}, f_{te2j} represent the complex velocities and forces for the jth mount and for the jth acoustic element on the radiating panel; and finally, v_{scj}, f_{scj}, and v_{rcj}, f_{rcj} represent the control system complex velocities and forces for the jth control force at the jth control point either on the source or radiating panels.

The dynamics of the source and radiating panels are modeled using a mobility matrix formulation so that velocity and force vectors can be expressed in the following form:

$$\boldsymbol{v}_s = \mathbf{Y}_{s1}\boldsymbol{f}_s + \mathbf{Y}_{s2}\boldsymbol{f}_p + \mathbf{Y}_{s3}\boldsymbol{f}_c \tag{15}$$

$$\boldsymbol{v}_r = \mathbf{Y}_{r1}\boldsymbol{f}_r + \mathbf{Y}_{r2}\boldsymbol{f}_f + \mathbf{Y}_{r3}\boldsymbol{f}_c \tag{16}$$

where $\mathbf{Y}_{s1}$, $\mathbf{Y}_{s2}$, $\mathbf{Y}_{s3}$, and $\mathbf{Y}_{r1}$, $\mathbf{Y}_{r2}$, $\mathbf{Y}_{r3}$ are mobility matrices of the source and the radiating panel, and $\boldsymbol{f}_p$, $\boldsymbol{f}_c$, $\boldsymbol{f}_f$ are the primary excitation vector, control force vector, and flanking excitation vector, respectively. The details of the mobility matrices used in Eqs. (15) and (16), and also of the mobility and impedance matrices introduced in the forthcoming part of the formulation, are defined in [25].

The primary and flanking excitation vector are given by

$$\boldsymbol{f}_p \equiv \begin{Bmatrix} f_{p1} \\ f_{p2} \\ \vdots \\ f_{pk} \end{Bmatrix} \tag{17}$$

$$\boldsymbol{f}_f \equiv \begin{Bmatrix} f_{f1} \\ f_{f2} \\ \vdots \\ f_{fk} \end{Bmatrix} \tag{18}$$

The flanking excitation vector $\boldsymbol{f}_f$ acting on the radiating panel could be caused by a subsystem connected to it or by an additional

flanking path connecting the source panel to the radiating panel. If the source plate is excited by a plane acoustic wave, the components of the primary excitation vector are determined by the pressure field generated by the plane wave over the surface of each element of the source panel:

$$f_{pj}(x_j, y_j, \omega) = l_{x,e} l_{y,e} P e^{-j(k_x x_j + k_y y_j)} \tag{19}$$

where P is the amplitude of the plane wave, which has a wave number in the x direction given by $k_x = k \sin(\theta) \cos(\phi)$ and a wave number in the y direction given by $k_y = k \sin(\theta) \sin(\phi)$, where k is the wave number, θ and ϕ are azimuthal and elevation angles, whereas x_j and y_j are coordinates of the geometrical center of the corresponding element of the source panel. The term $Pe^{-j(k_x x_j + k_y y_j)}$ in Eq. (19) is the pressure at the geometrical center of the element and the term $l_{x,e} l_{y,e}$ is the area of the element. Therefore, the acoustic excitation is modeled by assuming that the pressure field over the surface of an element can be approximated by the pressure at the center of the element.

The dynamics of the transmission system is given by the following expression:

$$\boldsymbol{f}_t = \mathbf{Z}_t \boldsymbol{v}_t \tag{20}$$

where $\mathbf{Z}_t$ is an impedance matrix of the transmission system [25]. The subsets in the $\mathbf{Z}_t$ matrix due to mounting system stiffness are diagonal. The subsets in the $\mathbf{Z}_t$ matrix due to acoustical coupling are fully populated because a velocity at one element will generate a force that is caused by pressure fluctuations at the centers of all the other elements of the source and radiating plates.

The source and radiating panel Eqs. (15) and (16) can be grouped together in one equation:

$$\boldsymbol{v}_{sr} = \mathbf{Y}_{sr1} \boldsymbol{f}_{sr} + \mathbf{Y}_{sr2} \boldsymbol{f}_{pf} + \mathbf{Y}_{sr3} \boldsymbol{f}_c \tag{21}$$

where the mobility matrices and the excitation vector have the form

$$\mathbf{Y}_{sr1} = \begin{bmatrix} \mathbf{Y}_{s1} & \mathbf{0} \\ \mathbf{0} & \mathbf{Y}_{r1} \end{bmatrix} \tag{22}$$

$$\mathbf{Y}_{sr2} = \begin{bmatrix} \mathbf{Y}_{s2} & \mathbf{0} \\ \mathbf{0} & \mathbf{Y}_{r2} \end{bmatrix} \tag{23}$$

$$\mathbf{Y}_{sr3} = \begin{bmatrix} \mathbf{Y}_{s3} \\ \mathbf{Y}_{r3} \end{bmatrix} \tag{24}$$

$$\boldsymbol{f}_{pf} = \begin{Bmatrix} \boldsymbol{f}_p \\ \mathbf{0} \end{Bmatrix} \tag{25}$$

where $\mathbf{0}$ is the appropriately sized vector/matrix of zeros, and the junction velocity and force vectors are given by

$$\boldsymbol{v}_{sr} \equiv \begin{Bmatrix} \boldsymbol{v}_s \\ \boldsymbol{v}_r \end{Bmatrix} \tag{26}$$

$$\boldsymbol{f}_{sr} \equiv \begin{Bmatrix} \boldsymbol{f}_s \\ \boldsymbol{f}_r \end{Bmatrix} \tag{27}$$

where $\boldsymbol{v}_{sr}$ and $\boldsymbol{f}_{sr}$ are, respectively, the source-radiating velocity vector and the source-radiating force vector. The source-radiating vectors are related to the corresponding coupling system vectors so as to satisfy the continuity (for the velocity vectors) and equilibrium (for the force vectors) principles at each junction:

$$\boldsymbol{v}_t = \boldsymbol{v}_{sr} \tag{28}$$

$$\boldsymbol{f}_t = -\boldsymbol{f}_{sr} \tag{29}$$

If Eqs. (28) and (29) are substituted into Eq. (20), the source-radiating force vector and force-radiating velocity vector can be related by

$$\boldsymbol{f}_{sr} = -\mathbf{Z}_t \boldsymbol{v}_{sr} \tag{30}$$

Substitution of Eq. (30) into Eq. (21) yields

$$\boldsymbol{v}_{sr} = \mathbf{Q}_{tp} \boldsymbol{f}_{pf} + \mathbf{Q}_{tc} \boldsymbol{f}_c \tag{31}$$

where the matrices $\mathbf{Q}_{tp}$ and $\mathbf{Q}_{tc}$ are given by

$$\mathbf{Q}_{tp} = (\mathbf{I} + \mathbf{Y}_{sr1} \mathbf{Z}_t)^{-1} \mathbf{Y}_{sr2} \tag{32}$$

$$\mathbf{Q}_{tc} = (\mathbf{I} + \mathbf{Y}_{sr1} \mathbf{Z}_t)^{-1} \mathbf{Y}_{sr3} \tag{33}$$

Equation (30) used with Eq. (31) gives the source-radiating force vectors

$$\boldsymbol{f}_{sr} = -\mathbf{Z}_t \mathbf{Q}_{tp} \boldsymbol{f}_{pf} - \mathbf{Z}_t \mathbf{Q}_{tc} \boldsymbol{f}_c \tag{34}$$

$$\boldsymbol{f}_{sr} = \mathbf{R}_{tp} \boldsymbol{f}_{pf} + \mathbf{R}_{tc} \boldsymbol{f}_c \tag{35}$$

where $\mathbf{R}_{tp}$ and $\mathbf{R}_{tc}$ are given by

$$\mathbf{R}_{tp} = -\mathbf{Z}_t \mathbf{Q}_{tp} \tag{36}$$

$$\mathbf{R}_{tc} = -\mathbf{Z}_t \mathbf{Q}_{tc} \tag{37}$$

The control velocity vector can also be expressed using the mobility method:

$$\boldsymbol{v}_c = \mathbf{Y}_{c1} \boldsymbol{f}_{sr} + \mathbf{Y}_{c2} \boldsymbol{f}_{pf} + \mathbf{Y}_{c3} \boldsymbol{f}_c \tag{38}$$

where the mobility matrices have the form

$$\mathbf{Y}_{c1} = \begin{bmatrix} \mathbf{Y}_{cs1} & \mathbf{0} \\ \mathbf{0} & \mathbf{Y}_{cr1} \end{bmatrix} \tag{39}$$

$$\mathbf{Y}_{c2} = \begin{bmatrix} \mathbf{Y}_{cs2} & \mathbf{0} \\ \mathbf{0} & \mathbf{Y}_{cr2} \end{bmatrix} \tag{40}$$

$$\mathbf{Y}_{c3} = \begin{bmatrix} \mathbf{Y}_{cs3} & \mathbf{0} \\ \mathbf{0} & \mathbf{Y}_{cr3} \end{bmatrix} \tag{41}$$

where $\mathbf{Y}_{cs1}$, $\mathbf{Y}_{cs2}$, $\mathbf{Y}_{cs3}$, and $\mathbf{Y}_{cr1}$, $\mathbf{Y}_{cr2}$, $\mathbf{Y}_{cr3}$ are mobility matrices of the source and the radiating panel at the control locations and $\mathbf{0}$ is an appropriately dimensioned matrix of zeros. A detailed description of the elements of these matrices can be found in [25].

Substitution of Eq. (35) into Eq. (38) yields

$$\boldsymbol{v}_c = \mathbf{T}_{cp} \boldsymbol{f}_{pf} + \mathbf{T}_{cc} \boldsymbol{f}_c \tag{42}$$

where $\mathbf{T}_{cp}$ and $\mathbf{T}_{cc}$ are given by

$$\mathbf{T}_{cp} = \mathbf{Y}_{c1} \mathbf{R}_{tp} + \mathbf{Y}_{c2} \tag{43}$$

$$\mathbf{T}_{cc} = \mathbf{Y}_{c1} \mathbf{R}_{tc} + \mathbf{Y}_{c3} \tag{44}$$

If the control force vector $\boldsymbol{f}_c$ is related to the control velocity vector $\boldsymbol{v}_c$ by means of a matrix of feedback control functions $\mathbf{H}$

$$\boldsymbol{f}_c = -\mathbf{H}\boldsymbol{v}_c \tag{45}$$

then the control velocities can be calculated using Eq. (42) as follows:

$$\boldsymbol{v}_c = (\mathbf{I} + \mathbf{T}_{cc}\mathbf{H})^{-1}\mathbf{T}_{cp}\boldsymbol{f}_{pf} \tag{46}$$

whereas the source and radiating panel forces are determined by Eq. (35). Finally, the source and radiating velocities can now be calculated using Eq. (21). Thus, at this point, for a given disturbance amplitude, it is possible to calculate the double plate velocity distribution.

Two principal metrics are used in the forthcoming analysis: the frequency spectrum of the double panel sound transmission ratio and the spectrum of the spatially averaged radiating panel kinetic energy. The radiated sound power can then be evaluated using the velocities of the radiating elements [15], which are a subset of $\boldsymbol{v}_{sr}$, Eq. (8), as

$$W(\omega) = \boldsymbol{v}_{re}^H \mathbf{R}\,\boldsymbol{v}_{re} \tag{47}$$

where $\mathbf{R}$ is the radiation resistance matrix [15] and $(\,)^H$ denotes the Hermitian transpose (the complex conjugate).

Kinetic energy of either the source or radiating panel can be calculated using the following expressions [15]:

$$E_s(\omega) = \frac{1}{4}\rho_s h_s l_{xe} l_{ye} \boldsymbol{v}_{se}^H \boldsymbol{v}_{se} \tag{48}$$

$$E_r(\omega) = \frac{1}{4}\rho_r h_r l_{xe} l_{ye} \boldsymbol{v}_{re}^H \boldsymbol{v}_{re} \tag{49}$$

where ρ_s, h_s, ρ_r, h_r are mass densities and thicknesses of the source and radiating panels, respectively.

Finally, the sound transmission ratio is calculated as the ratio of radiated sound power to incident sound power, so that

$$T(\omega) = \frac{W_r(\omega)}{W_i} \tag{50}$$

where $W_r(\omega)$ is the radiating sound power, determined according to Eq. (47). The sound power of the incident plane wave W_i can be calculated using the following expression [15]:

$$W_i = |P^2|\frac{l_x l_y}{2\rho c}\cos\theta \tag{51}$$

where P is the acoustical pressure of the incident wave [Eq. (19)] which is $P = 1$ Pa throughout this paper.

III. Parametric Study of Passive Sound Transmission

The primary aim of the parametric study is twofold. The first is to validate the model by comparing the simulations with other results obtained from well-established analytical models [5]. The second is to investigate how the vibroacoustic response varies when model parameters are changed. This type of study facilitates the interpretation of the physical phenomena for the airborne and structure-borne sound transmission through the panel.

For double partitions, important parameters can be the material properties of the panels, their dimensions, the distance between them, and the stiffness of elastic mounts which structurally connect the two plates. To perform a realistic study, the variation of these properties is selected with reference to materials and dimensions representative of an aircraft fuselage wall. The material properties and construction geometry of the bodywork of transportation vehicles are chosen by designers to meet functionality and safety requirements. In contrast, trim panels are designed for noise reduction and other constraints such as functionality, style, thermal insulation, etc. Therefore, for the purpose of the parametric study, the thickness and material of the radiating panel have been varied, whereas the source panel properties have been held fixed.

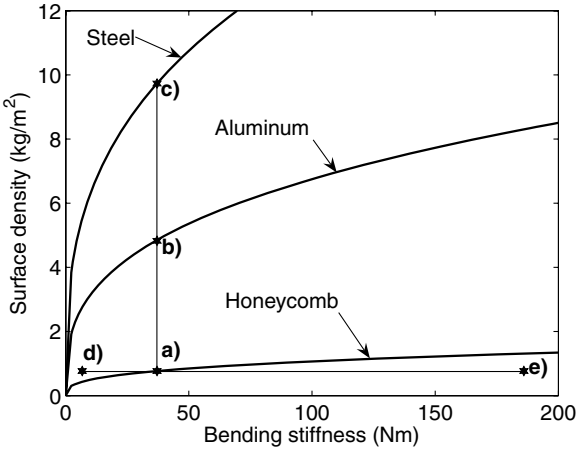

Fig. 3 Surface density and bending stiffness curves for three different radiating panel materials. Designs a–e are indicated in the density-stiffness plane.

Three different radiating panels have been investigated: 1) light and stiff polymer honeycomb plate, 2) heavier but less stiff aluminum plate, and 3) heavy steel plate with low stiffness. The bending stiffness of a rectangular isotropic plate is given by [26]

$$B = E\frac{h^3}{12} \tag{52}$$

where h is the thickness of the plate, and E is Young's modulus. The surface density of the plate (mass of the plate per unit area) is given by [26]

$$m = \rho h \tag{53}$$

where ρ is the mass density of the plate material. Thus, for a given material, the bending stiffness and surface density are linked by the following law:

$$B = \frac{E}{\rho^3}m \tag{54}$$

which is plotted in Fig. 3 for the three materials considered in this study.

Designs a, b, and c represent three materials with constant bending stiffness and surface density between 0.765 and 9.75 kg/m^2. Also, the effect of different bending stiffness of the radiating panel have been investigated, while keeping the surface density constant, as indicated by sets a, d, and e in Fig. 3. The remaining parameters that have been varied are the air gap thickness and the stiffness of the four elastic mounts. All variations considered are summarized in Table 1.

The column which contains the parameters of the reference case a is in bold. Asterisks indicate that the value of a parameter is the same as the referent case value given in column a. Table 2 gives the remaining parameters which were kept constant in all simulations.

A. Effects of the Radiating Panel Surface Density

The effects of the radiating panel surface density are analyzed considering the designs a, b, and c, indicated in Fig. 3. The three designs have the same radiating panel stiffness, but different surface densities, as listed in Table 1. The cavity depth for all the designs is 30 mm. The radiating panel kinetic energy per unit amplitude of the incident wave, Eq. (49), and the sound transmission ratio, Eq. (50), are plotted in Fig. 4 against the frequency.

Considering first the system design a, with the honeycomb radiating panel, below about 444 Hz, the kinetic energy and sound radiation are characterized by well-separated resonances. These resonances are due to the coupled response of the two panels via the four mounts and the air in the cavity. The cavity air acts as an additional distributed spring because the first cavity resonance occurs at about 415 Hz. Therefore, these resonances are

Table 1 Values of varied parameters

	a	b	c	d	e	f	g	h	i
Mount stiffness k_m, N/m	**5890**	*	*	*	*	*	*	0	58,900
Cavity depth l_z, m	**0.03**	*	*	*	*	0.02	0.04	*	*
Radiating panel bending stiffness B_r, Nm	**33.6**	*	*	6.72	168	*	*	*	*
Radiating panel surface density m_r, kg/m^2	**0.765**	4.81	9.75	*	*	*	*	*	*
Radiating panel Young's modulus E_r, Pa	$\mathbf{15 \cdot 10^9}$	$71 \cdot 10^9$	$210 \cdot 10^9$	N.A.	N.A.	*	*	*	*
Radiating panel mass density ρ_r, kg/m^3	**255**	2720	7800	N.A.	N.A.	*	*	*	*
Radiating panel thickness h_r, m	**0.003**	0.00177	0.00125	N.A.	N.A.	*	*	*	*

Table 2 Values of constant parameters

Radiating panel loss factor η_r	0.03
Air mass density ρ_{air}	1.19
Speed of sound c_0, m/s	343
Cavity modal damping ratio η_{air}	0.1
Source panel surface density m_s, kg/m^2	2.72
Source panel bending stiffness B_s, Nm	5.92
Source panel Young's modulus E_s, Pa	$71 \cdot 10^9$
Source panel mass density ρ_s, kg/m^3	2720
Source panel thickness h_s, m	0.001
Source panel loss factor η_s	0.02
Mount loss factor η_m	0.05

characterized by a plate–spring–plate type of coupled modes, where the source plate undergoes volumetric flexural deformations with deflection shapes similar to the (1, 1), (2, 1), (1, 2) modes of a simply supported plate. The radiating plate is characterized by volumetric rigid body deformations similar to a) the (0, 0) even mode, b) the (1, 0) and (0, 1) beam-type modes, and c) (1, 1), (2, 1), (1, 2) flexible modes of a freely suspended plate. Figures 5a and 5b depict the corresponding deflection shapes at the first and fifth resonant frequency, respectively. Note that the two plates move in phase because they are strongly coupled by the stiff distributed air spring, which forces the radiating plate to undergo motion similar to that of the source panel.

The kinetic energy plot in Fig. 4 is characterized by more resonances than the sound transmission ratio plot. This is due to the fact that the modes with small volumetric components (i.e., even–even or even–odd modes), such as the fifth mode (Fig. 5b), have small radiation efficiency. These resonances also have small amplitudes because the air coupling between the two panels is weaker when nonvolumetric modes are involved. At 444 Hz, there is a large amplitude resonance noticeable in either plot in Fig. 4. This resonance is usually referred to as the mass–air–mass resonance [5], and the deflection shape is characterized by out-of-phase motion of the two plates (Fig. 5c). Because for design a, the first cavity resonance occurs at 415 Hz, the cavity mode interferes with the shape of the mass–air–mass mode. At frequencies above the mass–air–mass resonance, the response is characterized by the typical mass law [5] with an initial decrement of the sound radiation of 18 dB per octave band. Also, the modal density at those frequencies is much higher because, together with the modes controlled by the two plates, there are also modes controlled by the cavity. Thus, the rising modal overlap effect and the increasing damping action on the two panels smooths out the spectra of the response and sound radiation which no longer shows well-separated, lightly damped resonance peaks.

According to the simplified model given by Fahy and Gardonio [5], the mass–air–mass resonant frequency for unbounded plates depends upon the surface densities of the two plates and the stiffness of the air. The air stiffness is determined by the cavity depth, air density, and speed of sound, such that

$$\omega_0 = \left[\left(\frac{\rho_{\text{air}} c_0^2}{l_z}\right)\left(\frac{m_s + m_r}{m_s \cdot m_r}\right)\right]^{0.5} \tag{55}$$

The mass–air–mass resonant frequency predicted by Eq. (55) is 423 Hz in this case, whereas the simulations show a value of 444 Hz. The simulated value can be considered in good agreement with theory, taking into account the fact that Eq. (55) is valid for infinite plates, coupled only by the air between them.

Above the mass–air–mass resonance, the sound transmission ratio is mass controlled so that the minima of the sound transmission ratio for this frequency range can be approximated using the following expression [5]:

$$T = -20\log\left[\frac{(m_s + m_r)\omega}{2\pi}\right] - 40\log\frac{\omega}{\omega_0} + 42 \tag{56}$$

which is valid up to a critical frequency [5]

$$\omega_c = \frac{10^{-1.8} \cdot \rho_{\text{air}} \cdot c_0^2}{2\pi l_z} \tag{57}$$

Above the critical frequency ω_c, the theoretical minima of the sound transmission ratio descend with a rate of 12 dB per octave band, following the equation [5]

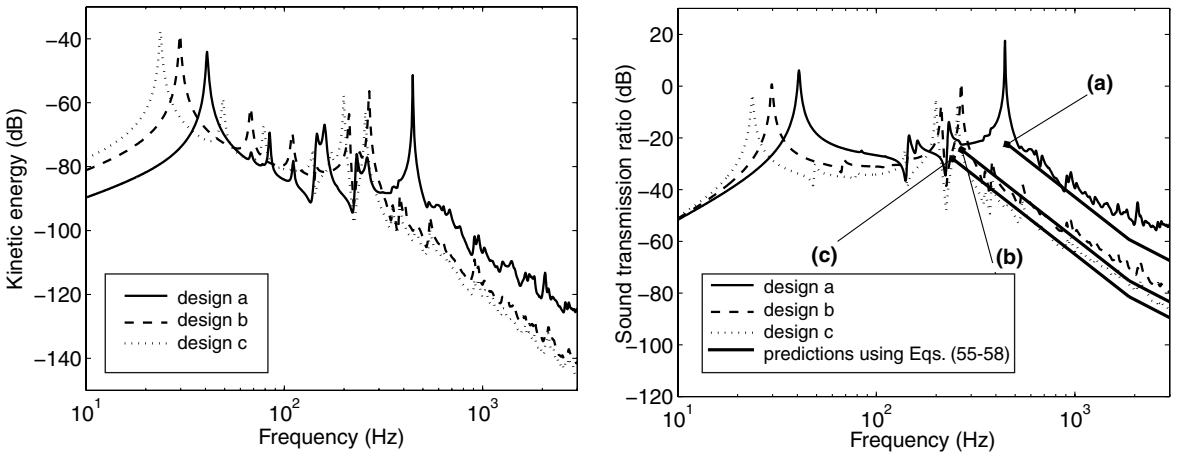

Fig. 4 Variation of the radiating panel surface density. Radiating panel kinetic energy (left-hand side), sound transmission ratio (right-hand side).

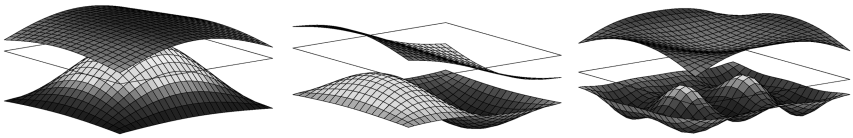

a) f=41 Hz b) f=84 Hz c) f=444 Hz

Fig. 5 Scaled deflection shapes at three different resonant frequencies.

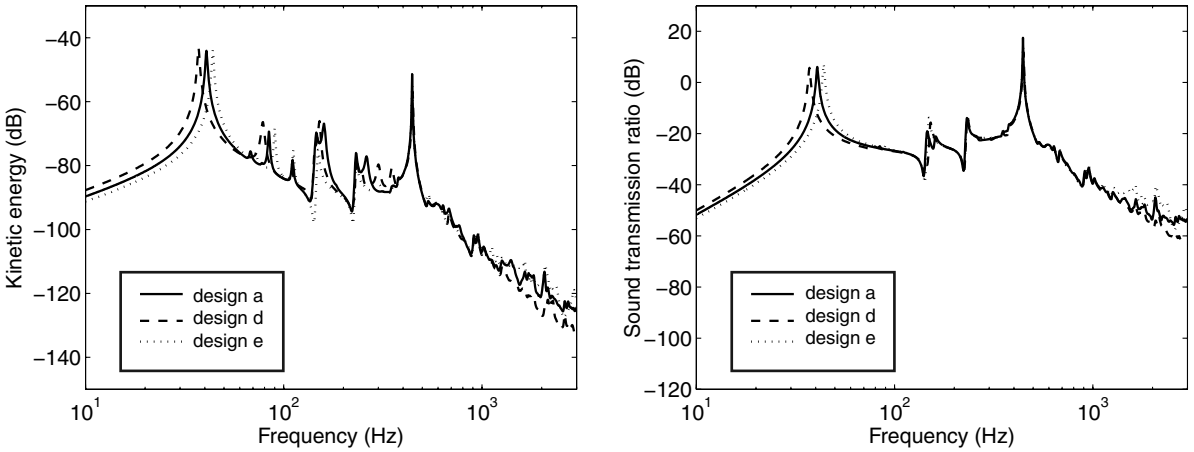

Fig. 6 Variation of the radiating panel bending stiffness. Radiating panel kinetic energy (left-hand side), sound transmission ratio (right-hand side).

$$T = -20\log\left(\frac{m_s \cdot \omega}{2\pi}\right) - 20\log\left(\frac{m_r \cdot \omega}{2\pi}\right) + 78 \qquad (58)$$

Considering now the aluminum and steel radiating panels, with the same bending stiffnesses but increased surface density, as shown by dashed and dotted lines in Fig. 4, the sound transmission ratio and the kinetic energy plots show a clear reduction of resonant frequencies as the surface density is increased. Also, the mean value of the sound transmission ratio decreases as the density per unit surface increases. This phenomenon shows a marked mass effect, because it affects both the coupled response of the double panel, as well as the sound radiation by the radiating panel. Predictions based on Eqs. (55–58) are shown on the sound transmission ratio plots with solid thick lines. Considering the mass variation effect of the radiating plate, there is good agreement between the simulated and the predicted mean sound transmission ratios.

B. Effects of the Radiating Panel Bending Stiffness

The effects of the radiating panel stiffness are analyzed considering designs a, d, and e indicated in Fig. 3, which have the same radiating panel density per unit area, but different bending stiffnesses, as listed in Table 1. The cavity depth for all the simulations was 30 mm. The radiating panel kinetic energy and the sound transmission ratio are shown in Fig. 6 against the frequency for the three cases.

Considering system designs d, e, and a, below about 440 Hz, the response and sound radiation are characterized by well-separated resonances just as observed in the previous subsection. The response and sound transmission ratio is also characterized by the mass law at the frequencies above about 440 Hz (the mass–air–mass mode). In fact, the natural frequency of this mode does not change with stiffness of the radiating plate. This is not a surprising outcome because the mode is mainly determined by out-of-phase motion of the two plates coupled by the air spring and, as Eq. (55) suggests, the natural frequency of the mode predominantly depends upon the two masses and the air spring stiffness. At frequencies above the mass–air–mass resonance, where the response is mass controlled, the sound transmission ratio is slightly higher for stiffer radiating panels.

Clear changes in the sound transmission ratio and kinetic energy also occur at lower frequencies, for example, below the first resonance of the coupled system (approximately 40 Hz), where the response is stiffness controlled. The natural frequency of the first mode tends to decrease as the stiffness of the radiating plate is decreased. Similar behavior occurs for all the resonant frequencies below the mass–air–mass resonance. The sound transmission ratio in the whole frequency band tends to decrease as the radiating plate stiffness decreases.

C. Effects of the Cavity Depth

The effect of cavity depth is shown in Fig. 7 for depths of 20, 30, and 40 mm. The stiffness of the mounts, as well as other double panel parameters, were kept constant, as listed in Table 1, according to designs f and g.

Both total kinetic energy and sound transmission ratio plots show little variation below the mass–air–mass resonant frequency as the air gap is increased. The principal variation occurs at the mass–air–mass resonance which decreases from 444 to 400 Hz as the cavity depth increases. This is because the air stiffness becomes smaller as the gap between the two panels increases. This cavity depth effect is in agreement with predictions based on Eq. (55).

On the other hand, the low-frequency response, for example, near the first resonant frequency (40 Hz), remains almost unaltered by the variation in the depth of the air cavity. This is because at such low frequencies, the cavity air is controlled by the 0, 0, 0 volumetric mode which behaves like an extremely stiff distributed spring. As a result, the modal stiffness of the 40 Hz mode remains unaltered with variations of the air gap, because it is predominantly determined by the stiffnesses of the two plates. The modal mass is barely affected by the increased mass of the cavity air (as the cavity depth increases), due to the relatively low air mass density. Simulation results are in agreement with predictions based on Eqs. (55–58), as shown on the sound transmission ratio plots by solid thick lines.

D. Effects of the Stiffness of the Mounting System

In general, the spectra of the radiating panel total kinetic energy and the sound transmission ratio show little variation as the stiffness of the four mounts is changed. The most important effect corresponds to the first system resonant frequency at about 40 Hz which, as shown in Fig. 8, tends to rise as the stiffness of the mounting system increases. This is due to the fact that, for soft mounts, the volumetric displacement of the source panel is absorbed by the rigid body

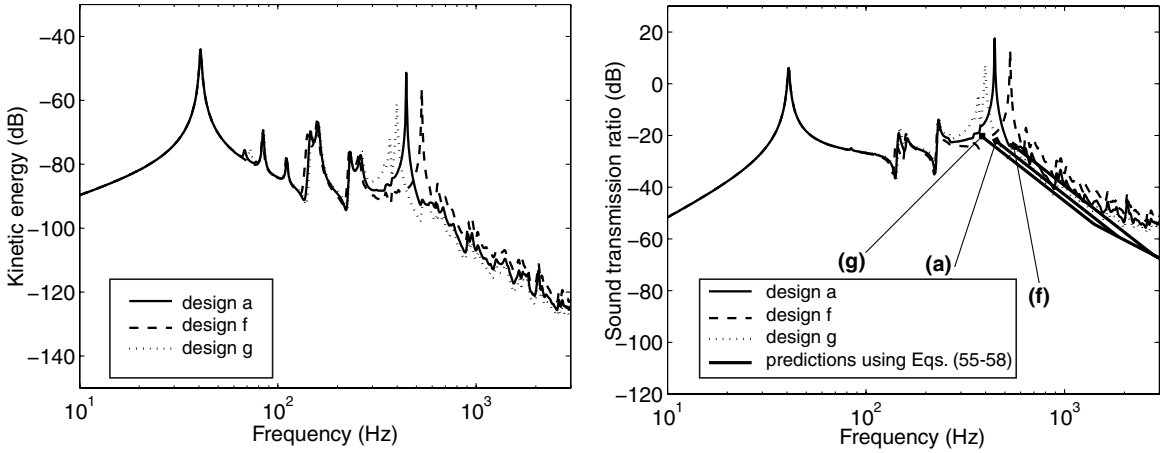

Fig. 7 Variation of the cavity depth. Radiating panel kinetic energy (left-hand side), sound transmission ratio (right-hand side).

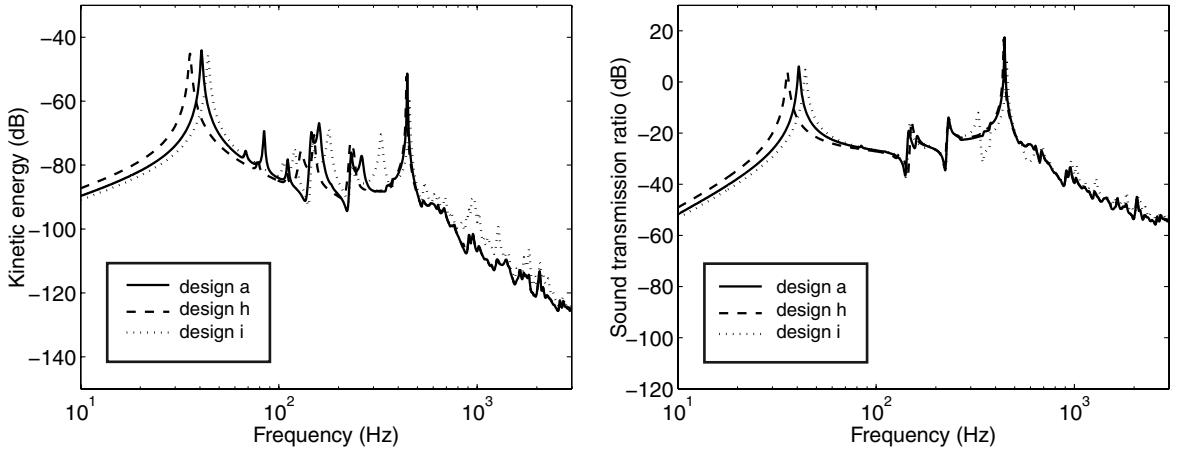

Fig. 8 Variation of the mount stiffness. Radiating panel kinetic energy (left-hand side), sound transmission ratio (right-hand side).

motion of the radiating panel, so that the modal stiffness is mainly determined by the stiffness of the source panel and the four mounts. In contrast, when stiff mounts are used, the volumetric displacement of the source panel is absorbed by the (1, 1) flexural mode of the radiating panel so that there is an effective increase in modal stiffness.

The mass–air–mass resonant frequency is affected slightly by the variation of the mount stiffness. The air stiffness effect is much more important and the modal stiffness contributed by the mounts is relatively small. Amplitudes of the sound transmission ratio and the radiating plate kinetic energy at the mass–air–mass resonance tend to decrease as the stiffness of the mounts is increased. This is probably due to the fact that more rigid mounts, located close to the simply supported boundary of the source panel, constrain the vibration of the radiating panel, especially its rigid body motion.

IV. Decentralized Direct Velocity Feedback Control

Direct velocity feedback control (DVFB), implemented using multi-input/multi-output decentralized loops, is considered in this section. The velocity sensors and force actuators are collocated, which guarantees unconditional stability of the feedback loops, if ideal sensors and actuators are assumed [14,15]. A direct velocity feedback control scheme is depicted in Fig. 9, which is unconditionally stable for passive plant response $\mathbf{T}_{cc}(\omega)$ and a passive controller $\mathbf{H}(\omega)$.

Four control arrangements are investigated in this section. The first two consist of a 4×4 array of decentralized velocity feedback control systems using collocated velocity sensors and idealized skyhook force actuators, either on the source or the radiating panels.

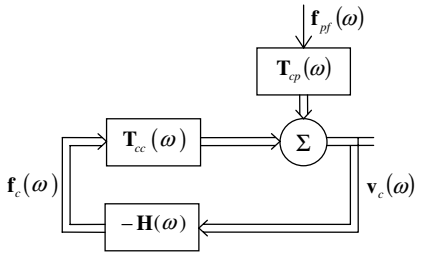

Fig. 9 Direct velocity feedback systems.

The third arrangement applies two 4×4 arrays of decentralized velocity feedback systems on the two panels simultaneously. The fourth control approach considers a 4×4 array of reactive actuators between the two panels, whereas the error signal is the relative velocity between the two panels at the control locations. Figure 10 schematically shows the four feedback arrangements.

Simulations for each control approach have been performed up to 3 kHz with different feedback gain levels. The material properties of the radiating panel correspond to design a (Table 1). The simulation results using the radiating panel active damping are depicted in Fig. 11 using three different feedback gain values. The left-hand plot shows kinetic energy of the radiating panel, whereas the right-hand plot shows the sound transmission ratio.

As the control gains are increased, the active damping action increases so that, as shown by the dashed lines, the response of the radiating panel, and thus the sound radiation, decreases at low radiating panel resonance frequencies. However, when very large

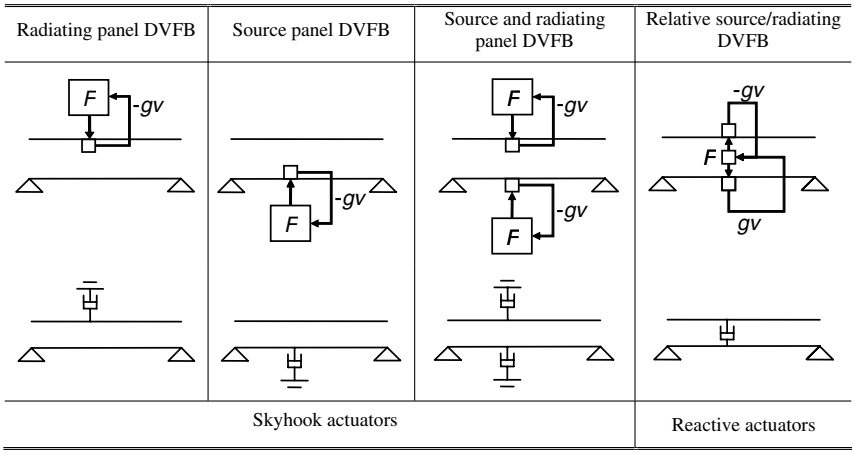

Fig. 10 Feedback arrangements.

control gains are used, large reductions of the radiating panel kinetic energy and sound transmission ratio are achieved at low frequencies, but there is an increase at higher frequencies, due to a pinning effect [15]. Similar studies carried out on single panels with a 4×4 array of decentralized velocity feedback control systems using collocated velocity sensors and point forces, have shown that when very large feedback gains are implemented, the pinning effect produces two consequences [15]. First, the response of the panel is governed by a new set of modes defined by the new pinning boundary conditions introduced by the feedback control loops. Second, the response is characterized by new lightly damped resonances occurring at higher frequencies, because the pinned control positions cannot generate any active damping. This type of phenomenon also occurs in this double panel case. Figure 11 illustrates the effect, showing the new resonances of the radiating panel which occur above approximately 1 kHz. In other words, the broadband sound transmission of the panel is increased for very high feedback gains, as will be demonstrated later in this section.

It must be emphasized that these results are valid provided the feedback control system is stable. This is indeed the case when collocated velocity sensors and ideal skyhook force actuators are used. When more practical actuators are used, for example, piezoelectric strain actuators or electrodynamic actuators that react against a proof mass or against the source panel, then stability is an open issue. As a result, the implementation of those feedback control gains which are necessary to get high reductions of the radiating panel kinetic energy and sound transmission ratio may be impossible.

The second approach implements MIMO direct velocity feedback on the source panel using skyhook forces. Simulation results are depicted in Fig. 12 for three different feedback gains. The left-hand plot shows the kinetic energy of the radiating panel, whereas the right-hand plot shows the sound transmission ratio.

As in the previous case, the response of the radiating panel and the sound transmission ratio decrease at the low-frequency resonances when the control gains are raised from zero. However, when very large control gains are implemented, although very large reductions are achieved at the first few resonance frequencies, the new lightly damped resonances become prominent around the mass–air–mass resonant frequency. Active damping of the source panel reduces neither the response nor the sound radiation near the mass–air–mass resonant frequency. This is probably because the radiating panel is free to vibrate despite the highly constrained source panel motion, because of the large volumetric deformations of the cavity air, as explained in Sec. III.A of this paper.

The plots in Fig. 13 show the control effects that result when the 4×4 array of skyhook active dampers act simultaneously on the source and radiating panels.

Comparing these results with those plotted for the control system acting on the radiating panel (Fig. 11), it is clear that relatively large control effects are generated when the two control systems act simultaneously. However, it must be emphasized that this is actually a 32 channel control system in comparison to the 16 channel control system of the first two arrangements. For very high feedback gains, there is still a pinning effect resulting in new lightly damped resonances above approximately 1 kHz.

The last control approach is concerned with 16 reactive actuators attached to the source and the radiating panels and driven by relative velocity feedback loops between the junction points of the actuators (Fig. 10). In practice, this could be realized by use of two velocity sensors per each actuator, as shown in Fig. 1, and by subtracting the two velocity signals to obtain the relative velocity. The reactive

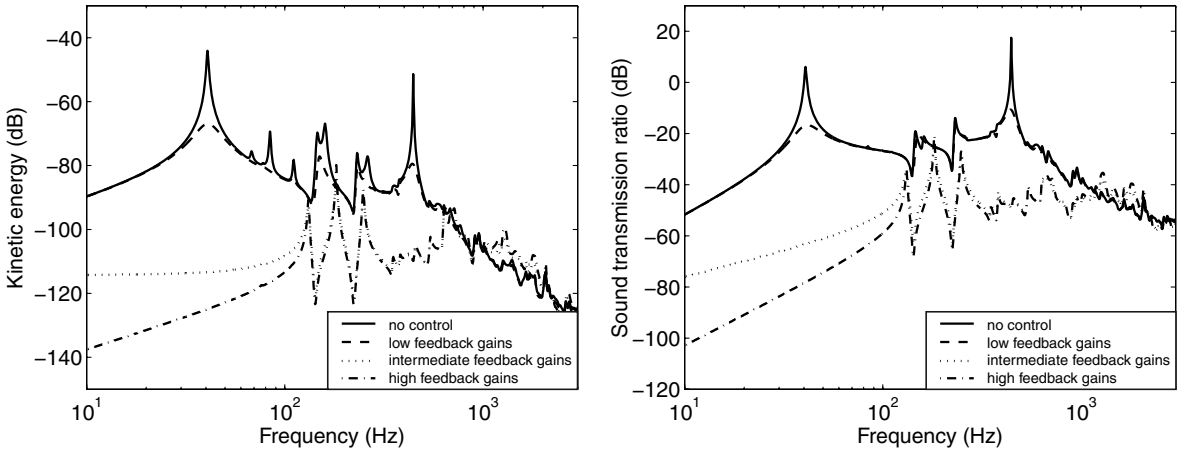

Fig. 11 Radiating panel direct velocity feedback using skyhook forces.

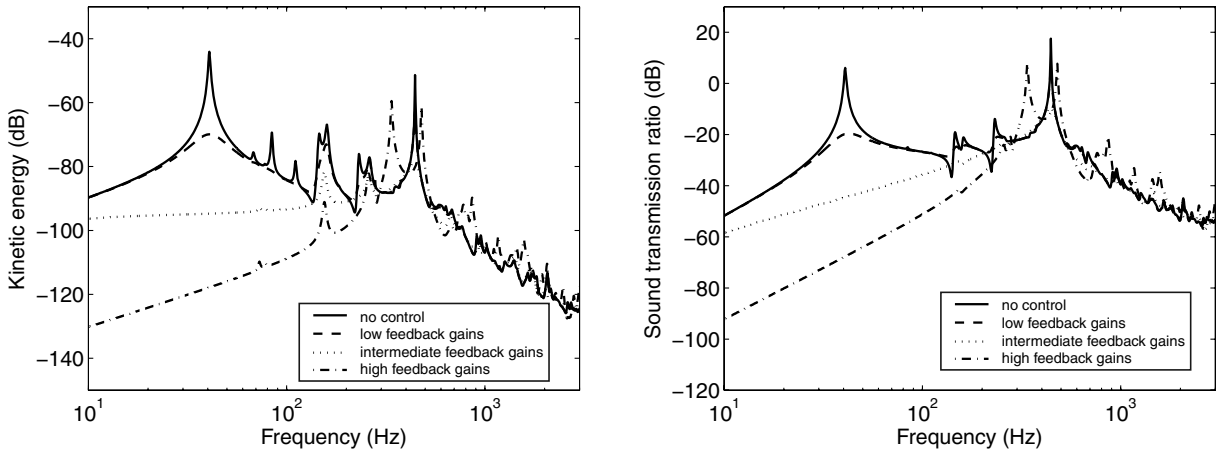

Fig. 12 Source panel direct velocity feedback using skyhook forces.

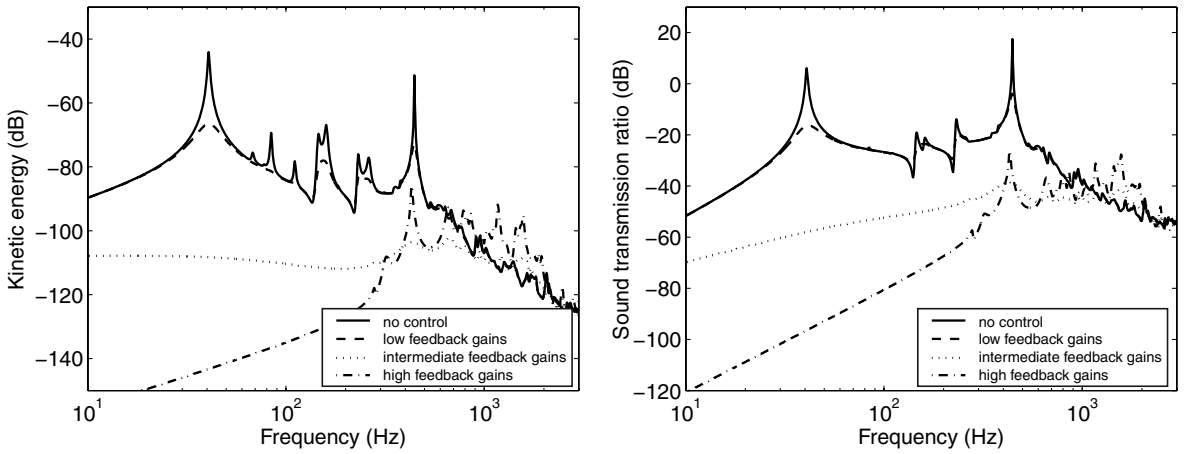

Fig. 13 Source and radiating panel velocity feedback using skyhook forces.

actuator could be implemented by attaching either end of an electrodynamic actuator to each plate. Neglecting actuator dynamics, an ideal reactive actuator is dual and collocated with a relative velocity sensor. This guarantees unconditional stability of the direct velocity feedback loop. Therefore, for this approach, a particular stability analysis is not needed, as long as ideal reactive actuators with ideal velocity sensors are considered.

The simulation of the control performance is depicted in Fig. 14 using three different feedback gains plus the open loop case.

As the control gains are raised from zero, active damping is generated, so that the response at the low-frequency resonances (below the mass–air–mass resonance) decreases. For intermediate feedback gains, as shown by dotted lines, large reductions in the resonant response and the sound transmission are obtained. However, comparing the plots in Fig. 14 to those in Figs. 11 and 13, the maximum control effectiveness that is obtained using intermediate gains is much lower. If very large control gains are implemented, the natural frequencies of the low-order modes are merely shifted up, without reductions in the resonant response and sound transmission. This is because, in this case, the two panels move together as if they were connected by an array of infinitely rigid studs, so that the double panel behaves like a thick and light single panel with a high stiffness–mass ratio. However, even in that case, the response and sound transmission at the mass–air–mass resonant frequency are significantly reduced. This is because the relative dampers successfully restrict the typical out-of-phase motion of the two plates (see Sec. III.A). However, above the mass–air–mass resonance, the sound transmission is increased by the control system and the beneficial mass law, Eq. (56), that governs the passive response is compromised.

The two plots in Fig. 15 show the kinetic energy of the radiating panel and the sound transmission ratio, integrated from 0 to 3 kHz and normalized with respect to the uncontrolled case, for the four analyzed control strategies: active damping of the radiating panel, active damping of the source panel, simultaneously applied radiating and source active damping, and relative active damping.

The results for the radiating panel control are represented by the dash-dotted lines in Fig. 15. Both the kinetic energy of the radiating panel and the sound transmission ratio monotonically decrease as the 16 control gains are raised, so that a maximum reduction, respectively, of about 29 and 32 dB are generated for the radiating panel active damping strategy (dash-dotted lines). For higher control gains, the reduction of kinetic energy and sound transmission ratio degrades because of the pinning effect that introduces a modal response characterized by new lightly damped resonances.

The overall reductions of the kinetic energy and sound transmission ratio in the case of source panel control are shown by the dashed lines in Fig. 15. The reductions are much lower in comparison to those obtained with the 16 channel control system on the radiating panel. In fact, the radiating panel kinetic energy is brought down by a maximum of about 17 dB, whereas the sound transmission ratio goes down by only 12 dB. In this case, for very large control gains, the pinning effect on the source panel rearranges the response of the double panel in such a way that the normalized sound transmission ratio is similar to that of the noncontrolled system.

The dotted lines in Fig. 15 show the control effects that would be generated when the two control arrangements act simultaneously on the source and radiating panels. Comparing these results with those plotted for the control system acting on the radiating panel, it is clear

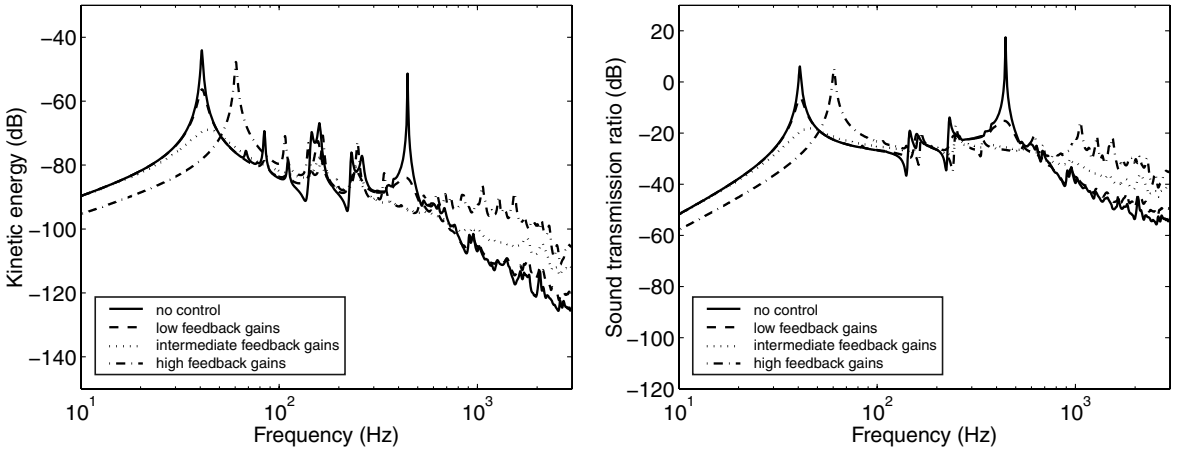

Fig. 14 Relative velocity feedback using reactive control actuators.

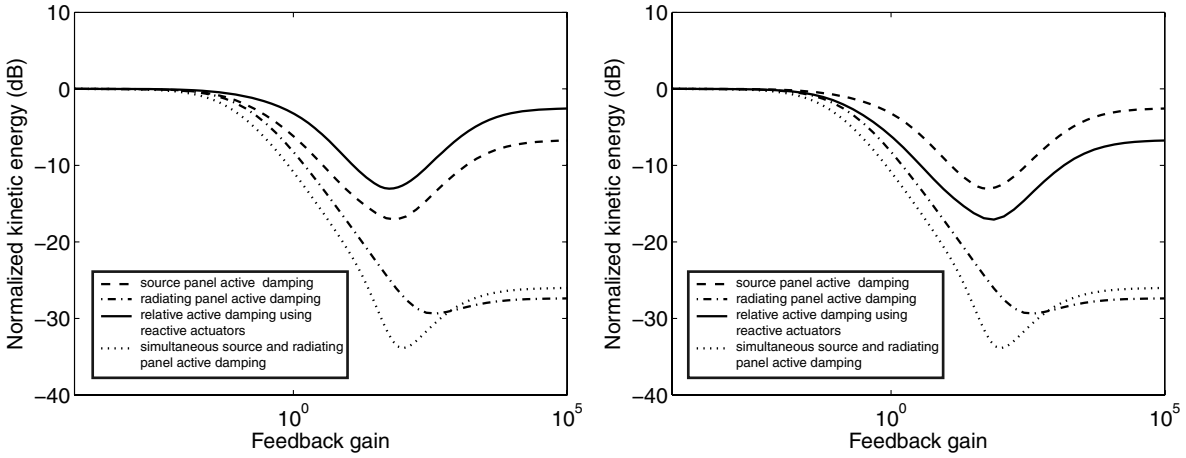

Fig. 15 Normalized kinetic energy of the radiating panel (left) and sound transmission ratio (right), integrated from 0 to 3 kHz.

that relatively large reductions are generated when the two control systems act simultaneously. However, the dotted lines in Fig. 15 indicate that the maximum reduction of the kinetic energy and the sound transmission ratio are increased only by a few dB. Thus, it may be possible to achieve much larger reductions by arranging the 32 control units on the radiating panel.

Finally, as shown by the solid lines in Fig. 15, for the case of reactive actuators driven by relative velocity signals, the maximum reductions of the radiating panel normalized kinetic energy and normalized sound transmission ratio are of about 13 and 18 dB. Although the reductions with skyhook control forces acting on the radiating panel are almost twice as much, the reactive actuators represent a more practical solution.

V. Conclusions

In this paper, a theoretical analysis is presented of a smart double panel system for active vibration control. The system consists of two panels coupled structurally by passive elastic mounts and acoustically by air in the cavity between the two panels. The principal dimensions of the double panel have been selected to replicate a simplified double wall fuselage of an aircraft. A parametric study has been performed which shows that, in general, the vibration and the sound transmission of the partition have frequency spectrums characteristic for double panels. This means that below the mass–air–mass resonant frequency, the response and the sound transmission spectra are characterized by well-separated resonances. On the other hand, the radiating panel kinetic energy and sound transmission ratio are governed by a mass law at frequencies above the mass–air–mass resonant frequency. The cases studied show that when the (surface density)/(bending stiffness) ratio increases, the response of the radiating panel and sound transmission is affected by a downward shift of the resonant frequencies. Variations of cavity depth tend to shift the mass–air–mass resonance frequency, whereas variations of the mount stiffness tend to shift the lowest resonance frequency of the double panel.

The effects of four MIMO decentralized feedback control systems for the reduction of the low-frequency sound transmission were considered. The overall conclusion is that skyhook damping on the radiating panel produced the largest broadband reductions of both the radiating panel kinetic energy and the sound transmission ratio: up to 29 and 32 dB, respectively. The skyhook damping on the source panel produced modest results of 17 and 12 dB broadband reductions of radiating panel kinetic energy and sound transmission ratio. The use of skyhook active damping on both panels increased the kinetic energy and sound transmission reductions by just few decibels in comparison to the radiating panel active damping. Finally, the implementation of relative damping produced 13 and 18 dB reductions of radiating panel kinetic energy and sound transmission ratio. Although the radiating panel skyhook control produces the best reductions, the reactive actuation scheme is a more realistic strategy than the skyhook actuation, thus the latter can be considered as a promising strategy. However, the feedback gains should be chosen so as to avoid pinning of the two plates, because it prevents the generation of active damping at the low frequencies and compromises good sound transmission loss at higher frequencies.

Acknowledgments

The theoretical work presented in this paper has been performed by Neven Alujević within the European Doctorate in Sound and

Vibration Studies, which is supported by the European Commission through the Marie Curie Early Stage Training Fellowships.

References

[1] Mixson, J. S., and Wilby, J. S., *Interior Noise*, edited by Hubbard, H. H., Aeroacoustics of Flight Vehicles, Theory and Practice, NASA Langley Research Center, Hampton, VA, 1995, Chap. 16, pp. 271–335.

[2] Fahy, F. J., *Fundamentals of Noise and Vibration Control*, edited by Fahy, F. J., and Walker, J. G., Fundamentals of Noise and Vibration, E & FN Spon, London, 1998, Chap. 5, pp. 225–309.

[3] Brennan, M. J., and Ferguson, N. S., *Vibration Control*, edited by Fahy, F. J., and Walker, J. G., Advanced Applications in Acoustics, Noise and Vibration, E & FN Spon, London, 2004, Chap. 12, pp. 530–580.

[4] Fahy, F. J., *Engineering Acoustics*, Academic Press, London, 2001.

[5] Fahy, F. J., and Gardonio, P., *Sound and Structural Vibration*, Elsevier, London, 2006.

[6] Maury, C., Gardonio, P., and Elliott, S. J., "Model for Active Control of Flow-Induced Noise Transmitted Through Double Partitions," *AIAA Journal*, Vol. 40, No. 6, 2002, pp. 1113–1121.

[7] Fuller, C. R., Elliott, S. J., and Nelson, P. A., *Active Control of Vibration*, Academic Press, London, 1996.

[8] Gardonio, P., "Review of Active Techniques for Aerospace Vibro-Acoustic Control," *Journal of Aircraft*, Vol. 39, No. 2, March–April 2002, pp. 206–214.

[9] Nelson, P. A., and Elliott, S. J., *Active Control of Sound*, Academic Press, London, 1992.

[10] Elliott, S. J., *Signal Processing for Active Control*, Academic Press, London, 2001.

[11] Preumont, A., *Vibration Control of Active Structures*, Kluwer Academic, Norwell, MA, 2002.

[12] Clark, R. L., Saunders, W. R., and Gibbs, G. P., *Adaptive Structures*, 1st ed., Wiley, New York, 2002.

[13] Petitjean, B., and Legrain, I., "Feedback Controllers for Active Vibration Suppression," *Journal of Structural Control*, Vol. 3, Nos. 1–2, June 1996, pp. 111–127.

[14] Balas, M. J., "Direct Velocity Control of Large Space Structures," *Journal of Guidance and Control*, Vol. 2, No. 3, 1979, pp. 252, 253.

[15] Gardonio, P., Bianchi, E., and Elliott, S. J., "Smart Panel with Multiple Decentralised Units for the Control of Sound Transmission, Part 1: Theoretical Predictions; Part 2: Design of the Decentralised Control Units; Part 3: Control System Implementation," *Journal of Sound and Vibration*, Vol. 274, Nos. 1–2, 2004, pp. 163–232. doi:10.1016/j.jsv.2003.05.004

[16] Elliott, S. J., Gardonio, P., Sors, T. C., and Brennan, M. J., "Active Vibroacoustic Control with Multiple Local Feedback Loops," *Journal of the Acoustical Society of America*, Vol. 111, No. 2, 2002, pp. 908–915. doi:10.1121/1.1433810

[17] Gardonio, P., and Elliott, S. J., "Modal Response of a Beam with Sensor-Actuator Pair for the Implementation of Velocity Feedback Control," *Journal of Sound and Vibration*, Vol. 284, Nos. 1–2, 2005, pp. 1–22. doi:10.1016/j.jsv.2004.06.018

[18] Sun, J. Q., "Some Observations on Physical Duality and Collocation of Structural Control Sensors and Actuators," *Journal of Sound and Vibration*, Vol. 194, No. 5, 1996, pp. 765–770. doi:10.1006/jsvi.1996.0394

[19] Jayachandran, V., and Sun, J. Q., "Unconditional Stability Domains of Structural Control Systems Using Dual Actuator-Sensor Pairs," *Journal of Sound and Vibration*, Vol. 208, No. 1, 1997, pp. 159–166. doi:10.1006/jsvi.1997.1177

[20] Gardonio, P., Lee, Y. S., Elliott, S. J., and Debost, S., "Analysis and Measure of a Matched Volume Velocity Sensor and Uniform Force Actuator for Active Structural Acoustic Control," *Journal of the Acoustical Society of America*, Vol. 110, No. 6, Dec. 2001, pp. 3025–3031. doi:10.1121/1.1412448

[21] Meirovitch, L., *Dynamics and Control of Structures*, Wiley, New York, 1990.

[22] Paulitsch, C., Gardonio, P., and Elliott, S. J., "Active Vibration Control Using an Inertial Actuator with Internal Damping," *Journal of the Acoustical Society of America*, Vol. 119, No. 4, April 2006, pp. 2131–2140. doi:10.1121/1.2141228

[23] Benassi, L., and Elliott, S. J., "Active Vibration Isolation Using an Inertial Actuator with Local Displacement Feedback Control," *Journal of Sound and Vibration*, Vol. 278, Nos. 4–5, 2004, pp. 705–724. doi:10.1016/j.jsv.2003.10.065

[24] Elliott, S. J., Serrand, M., and Gardonio, P., "Feedback Stability Limits for Active Isolation Systems with Reactive and Inertial Actuators," *Journal of Vibration and Acoustics*, Vol. 123, No. 2, 2001, pp. 250–261. doi:10.1115/1.1350822

[25] Alujević, N., Frampton, K. D., and Gardonio, P., "Smart Double Panel with Decentralised Active Dampers for Control of Sound Transmission," Inst. of Sound and Vibration Research, TM 972, Southampton, England, U.K., 2007.

[26] Cremer, L., Heckl, M., and Ungar, E. E., *Structure-Borne Sound*, Springer–Verlag, Berlin, 1988.

M. Ahmadian
Associate Editor